energies

MDPI

Article

Projection-Based Coordinated Scheduling of Distribution–Microgrid Systems Considering Frequency Security Constraints

Xingwang Song [1], Lingxu Guo [2], Mingjun Sun [1], Xinyu Tong [1], Wei Wei [3,*] and Mengyu Liu [3,*]

[1] State Grid Tianjin Chengxi Electric Power Supply Branch, Tianjin 300110, China; xingwang.song@tj.sgcc.com.cn (X.S.); mingjun.sun@tj.sgcc.com.cn (M.S.); xinyu.tong@tj.sgcc.com.cn (X.T.)
[2] State Grid Tianjin Electric Power Company, Tianjin 300010, China; lingxu.guo@tj.sgcc.com.cn
[3] Key Laboratory of Smart Grid of Ministry of Education, Tianjin University, Tianjin 300072, China
* Correspondence: weiw@tju.edu.cn (W.W.); lmy320_@tju.edu.cn (M.L.)

Abstract

With the rapid development of distribution–microgrid (DN–MG) systems, they have become increasingly important in the construction of modern power systems. However, existing scheduling approaches often overlook the frequency security risks faced by microgrids when transitioning into unintentional islanding during contingencies. To address this issue, this paper proposes a projection-based coordinated scheduling method for DN–MG systems under microgrid frequency security constraints. First, an approximate frequency response curve is derived to characterize the maximum frequency deviation of microgrids after unintentional islanding, which is explicitly embedded into the microgrid optimization model to ensure frequency security. Second, to achieve efficient coordination, a power–energy boundary-based feasible region approximation is proposed for microgrids, which accurately characterizes the projection feasible region under inter-temporal coupling while reducing conservativeness. This enables a non-iterative coordination framework. Finally, case studies on a modified IEEE 33-bus system containing three microgrids demonstrate that the proposed method effectively limits the maximum frequency deviation to within 0.5 Hz, while the projection-based feasible region achieves 87.62% coverage, which is twice that of conventional box approximations. Overall, the proposed method ensures microgrid frequency security while balancing computational efficiency and privacy protection, highlighting its strong potential for practical engineering applications.

Keywords: distribution–microgrid system; frequency constraint; feasible region; coordinated scheduling

check for updates

Academic Editor: José Matas

Received: 25 September 2025
Revised: 14 October 2025
Accepted: 17 October 2025
Published: 30 October 2025

Citation: Song, X.; Guo, L.; Sun, M.; Tong, X.; Wei, W.; Liu, M. Projection-Based Coordinated Scheduling of Distribution–Microgrid Systems Considering Frequency Security Constraints. *Energies* **2025**, *18*, 5707. https://doi.org/10.3390/en18215707

Copyright: © 2025 by the authors. Licensee MDPI, Basel, Switzerland. This article is an open access article distributed under the terms and conditions of the Creative Commons Attribution (CC BY) license (https://creativecommons.org/licenses/by/4.0/).

1. Introduction

Microgrids, as key carriers of high-penetration distributed resources enabling local balance and flexible interaction, have been widely deployed in distribution networks [1,2]. They offer multiple advantages, including local consumption, enhanced resilience, black-start capability, and orderly grid-connection/disconnection [3]. However, as the scale and number of microgrids increase, independently optimizing distribution and microgrid subsystems cannot simultaneously ensure system-wide economic efficiency and operational security. Therefore, it is crucial to coordinate DN–MG systems in a way that satisfies operational constraints while fully leveraging the flexibility and support capabilities of microgrids [4].

Most existing DN–MG coordination methods primarily focus on minimizing economic costs. For instance, Ref. [5] proposes a steady-state convex bi-directional converter model-based optimization framework to enable high-efficiency economic dispatch of hybrid AC/DC networked MGs, while paying insufficient attention to the operational security of microgrids. In particular, during unintentional islanding events, low-inertia and power-electronic–dominated microgrids are prone to severe frequency deviations [6]. Several studies have proposed preventive scheduling strategies. For instance, Ref. [7] develops a minimum inertia evaluation framework under grid-connected and islanded conditions to guide secure operation; Ref. [8] derives frequency security constraints using finite differences, which capture both high- and low-frequency issues but yield nonconvex scheduling models with high computational burdens; Ref. [9] analytically derives maximum frequency deviation constraints with demand response under linearized primary frequency response assumptions, which oversimplify the dynamic differences among resources; Ref. [10] validates frequency security through time-domain simulations and introduces heuristic cuts to link simulation and optimization, but scalability and privacy concerns limit practical deployment.

Due to privacy concerns and the large amount of data exchanged among multiple microgrids, centralized coordination of DN–MG systems is generally impractical. Consequently, distributed optimization frameworks have been developed to achieve coordination while preserving autonomy. Among them, the Alternating Direction Method of Multipliers (ADMM) has emerged as a representative paradigm. Prior studies include the application of decentralized ADMM to demand-side clusters in optimal power flow problems [11], adaptive parameter-updating strategies for accelerating ADMM convergence [12], and extensions of ADMM to mixed-integer optimization problems [13]. However, these decentralized approaches typically require multiple communication rounds and extensive data exchange, which can lead to convergence delays or even algorithmic stalling.

To overcome these bottlenecks, dimension-reduced projection-based methods have recently been explored as a hierarchical yet non-iterative alternative. By mapping high-dimensional inter-temporal feasible regions into low-dimensional boundary-variable subspaces, each microgrid can submit only its projected feasible region, thereby enabling near non-iterative coordination and enhanced privacy protection. Although vertex-search-based projection methods [4] can approximate aggregated feasible regions for microgrid clusters, they suffer from combinatorial explosion in multi-period scenarios, limiting both accuracy and scalability. Multi-parametric programming [14–16] can, in principle, exactly characterize projection regions but is highly sensitive to parameter dimensionality. Meanwhile, robust optimization-based adaptive constraint generation [17] incrementally identifies critical operating points and constructs feasible cuts, but its computational complexity increases exponentially with the number of iterations. Therefore, efficiently constructing microgrid projection feasible regions under temporal coupling remains a key open challenge for achieving scalable and privacy-preserving coordination.

To overcome these challenges, this paper proposes a projection-based coordinated scheduling method for DN–MG systems under microgrid frequency security constraints. The main contributions are as follows: (1) an approximate frequency response curve is developed to characterize the primary frequency response of conventional generators and inverter-based resources in microgrids, from which linear maximum frequency deviation constraints are derived and embedded into the scheduling model; (2) a microgrid feasible region inner-approximation method is introduced, which leverages predefined geometric shapes and a leader–follower game to iteratively contract infeasible boundaries while preserving tractability.

The remainder of this paper is organized as follows. Section 2 presents the frequency security modeling approach. Section 3 formulates the DN–MG coordinated scheduling model. Section 4 develops the microgrid feasible region approximation method. Section 5 provides case studies, and Section 6 concludes the paper.

2. Modeling Frequency Security Constraints via Frequency Response Curves Approximation

2.1. Frequency Dynamics

Given the short electrical distances within a microgrid, the spatial–temporal distribution of frequency can be neglected, and the analysis is conducted with respect to the center of inertia frequency [18–20]. During unintentional islanding events, the frequency dynamics of a microgrid can be modeled by the following swing equation:

$$\frac{2H}{f_0}\frac{\mathrm{d}\Delta f(\tau)}{\mathrm{d}\tau} + D\Delta f(\tau) = \Delta P(\tau) - \Delta P^{\mathrm{dis}} \tag{1}$$

where H denotes the system inertia of the islanded microgrid; f_0 represents the nominal frequency; $\Delta f(\tau)$ denotes the frequency deviation; D is the system damping coefficient; $\Delta P(\tau)$ corresponds to the primary frequency response power output; ΔP^{dis} indicates the power imbalance, which in this paper refers to the power exchanged through the DN–MG interconnection line prior to the unintentional islanding event; and τ denotes the frequency response time. For clarity of exposition, the subsequent derivation focuses on the low-frequency case, in which ΔP^{dis} is positive and $\Delta f(\tau)$ is negative.

During the primary frequency regulation stage, $\Delta P(\tau)$ dynamically adjusts in response to the frequency deviation $\Delta f(\tau)$. The physical relationship can be modeled as a negative feedback system described by the following set of differential equations [21]:

$$\begin{cases} \Delta P(\tau) = \sum\limits_{i=1}^{N} \Delta P_i(\tau) \\ T_i \dfrac{\mathrm{d}\Delta P_i(\tau)}{\mathrm{d}\tau} + \Delta P_i(\tau) = -K_i \Delta f(\tau) \end{cases} \tag{2}$$

where i and N denote the index and the total number of primary frequency regulation units, respectively; $\Delta P_i(\tau)$ represents the primary frequency response power output of unit i; and K_i and T_i correspond to the droop gain and the time constant of unit i, respectively.

2.2. Frequency Constraint Modeling Based on Frequency Response Curves

Based on Equation (2) and the swing Equation (1), it can be observed that as the number of primary frequency regulation units N increases, the order of Equation (1) correspondingly rises. This makes the analytical derivation of the frequency deviation function $\Delta f(\tau)$ increasingly intractable, which is unfavorable for constructing subsequent frequency constraints. To address this issue, a frequency response curve construction method [22] is employed, whereby the frequency deviation function in Equation (2) is approximated by a quadratic function:

$$\Delta \hat{f}(\tau) = a\tau^2 + b\tau + c \tag{3}$$

where $\Delta \hat{f}(\tau)$ satisfies the following conditions: (1) the initial value is 0; (2) the initial slope equals the initial rate of change of $\Delta f(\tau)$; and (3) the minimum value is $-\Delta f_{\max}$, where

$\Delta f_{\max}$ is a positive constant representing the frequency deviation limit. Based on these conditions, the expressions for a, b, and c are given as follows:

$$\begin{cases} a = \frac{\Delta f_{\max}}{(\tau^*)^2}\tau^2 \\ b = -\frac{2\Delta f_{\max}}{\tau^*}\tau \\ c = 0 \\ \tau^* = \frac{4H\Delta f_{\max}}{\Delta P^{\text{dis}} f_0} \end{cases} \tag{4}$$

where τ^* denotes the estimated time at which the maximum frequency deviation occurs.

By substituting Equations (3) and (4) into Equation (2), the primary frequency response power output can be expressed as follows when the frequency deviation reaches the specified threshold:

$$\Delta\hat{P}(\tau^*) = \sum_{i=1}^{N} 2T_i K_i \Delta f_{\max}\left[\frac{1+\frac{2T_i}{\tau^*}}{2T_i} - \frac{T_i+\tau^*}{(\tau^*)^2}\left(1-e^{-\frac{\tau^*}{T_i}}\right)\right] \tag{5}$$

According to the equivalent condition of the maximum frequency deviation constraint proposed in [23], when the frequency deviation reaches the threshold, if the sum of the primary frequency response power and the damping power is greater than or equal to the power imbalance, the frequency deviation will no longer increase, thereby satisfying the maximum frequency deviation constraint. This relationship can be expressed as follows:

$$\Delta\hat{P}(\tau^*) + D\Delta f_{\max} \geq \Delta P^{\text{dis}} \tag{6}$$

2.3. Derivation of Linear Maximum Frequency Deviation Constraint

In constraint (6), the primary frequency response power $\Delta\hat{P}(\tau^*)$ contains an exponential function and therefore does not satisfy linear constraint conditions. To address this, a monotonicity analysis of $\Delta\hat{P}(\tau^*)$ is conducted, from which it can be obtained that the function is increasing with respect to $\Delta\hat{P}(\tau^*)$, while τ^* satisfies the following condition:

$$\tau^* = \frac{2\Delta f_{\max}}{\frac{\Delta P^{\text{dis}} f_0}{2H}} \geq \frac{2\Delta f_{\max}}{\overline{RoCoF}} \tag{7}$$

where $\overline{RoCoF}$ is the limit of rate of change in frequency.

According to Equation (7), τ^* has a lower bound, and therefore $\Delta\hat{P}(\tau^*)$ attains a minimum value. By taking $\Delta\hat{P}\left(2\Delta f_{\max}/\overline{RoCoF}\right)$ as a conservative estimate of $\Delta\hat{P}(\tau^*)$, the maximum frequency deviation constraint can be reformulated in a linear form as follows:

$$\Delta\hat{P}\left(2\Delta f_{\max}/\overline{RoCoF}\right) + D\Delta f_{\max} \geq \Delta P^{\text{dis}} \tag{8}$$

In addition, a frequency ramping rate constraint is incorporated as follows:

$$\frac{\Delta P^{\text{dis}} f_0}{2H} \leq \overline{RoCoF} \tag{9}$$

3. Coordinated Scheduling Model of Distribution–Microgrid Systems

3.1. Objective Function

In the coordinated scheduling problem considered in this paper, focus is placed on the construction of the microgrid projection feasible region, while the operating cost of

individual microgrids is not taken into account [24,25]. The objective of the coordinated scheduling model is to minimize the total operating cost of the distribution network:

$$\min \sum_{t\in T}\sum_{g\in G} c_g^{\mathrm{GEN}} P_{g,t}^{\mathrm{GEN}} + \sum_{t\in T}\sum_{e\in E}\left(c_e^{\mathrm{dch}} P_{e,t}^{\mathrm{dch}} + c_e^{\mathrm{ch}} P_{e,t}^{\mathrm{ch}}\right) + \sum_{t\in T} c_t^{\mathrm{EX}} P_t^{\mathrm{EX}} \tag{10}$$

where t and T denote the index and the set of scheduling periods, respectively; c_g^{GEN} and $P_{g,t}^{\mathrm{GEN}}$ represent the cost coefficient and the active power output of generator g; c_e^{dch} and c_e^{ch} denote the discharging and charging cost coefficients of the energy storage system, respectively; $P_{e,t}^{\mathrm{dch}}$ and $P_{e,t}^{\mathrm{ch}}$ are its discharging and charging power outputs; c_t^{EX} denotes the electricity price; and P_t^{EX} represents the exchanged power between the distribution network and microgrids.

3.2. Operation Constraints of DN

In the distribution network, generator constraints include capacity limits and ramping constraints, while energy storage constraints cover power–energy relationships. The power flow constraints of the distribution network are described using the DistFlow second-order cone model, and their detailed formulations can be found in [26]. In this paper, the set $\phi(\mathbf{x}_{\mathrm{DN}}) \le \mathbf{0}$ is used to represent the internal constraints of the distribution network, with $\mathbf{x}_{\mathrm{DN}}$ denoting the distribution network decision variables, and $\mathbf{x}_{\mathrm{DN,bd}} = \mathbf{x}_{\mathrm{MG,bd}}$ is introduced to represent the boundary coupling constraints between the distribution network and the microgrids.

3.3. Operation Constraints of MG

Let M and m denote the set and the index of microgrids, respectively. For each microgrid m, its operating constraints include the capacity constraint (11) and ramping constraint (12) of distributed generators, the power–energy constraints of distributed energy storage (13) and (14), the constraints of distributed renewable units (15), the power balance constraint (16), the maximum frequency deviation constraints (17)–(22), and the frequency ramping rate constraint (23).

$$p_i^{\min} \le p_{i,t} \le p_i^{\max}, \forall i \in G(m), t \in T \tag{11}$$

$$r_i^{\min} \le p_{i,t} - p_{i,t-1} \le r_i^{\max}, \forall i \in G(m), t \in T \tag{12}$$

$$p_i^{\mathrm{E,min}} \le p_{i,t}^{\mathrm{E}} \le p_i^{\mathrm{E,max}}, \forall i \in E(m), t \in T \tag{13}$$

$$E_{i,t}^{\min} \le \sum_{j=1}^{t} p_{i,j}^{\mathrm{E}} \le E_{i,t}^{\max}, \forall i \in E(m), t \in T \tag{14}$$

$$0 \le p_{i,t}^{\mathrm{R}} \le p_{i,t}^{\mathrm{Fore}}, \forall i \in W(m), t \in T \tag{15}$$

$$\sum_{i\in G(m)} p_{i,t} + \sum_{i\in E(m)} p_{i,t}^{\mathrm{E}} + \sum_{i\in W(m)} p_{i,t}^{\mathrm{R}} + p_{m,t}^{\mathrm{DM}} = P_t^{\mathrm{D}}, \forall t \in T \tag{16}$$

$$R_m^{+} + D_m \Delta f_{\max} \ge p_{m,t}^{\mathrm{DM}} \tag{17}$$

$$R_m^{+} \le \Delta \hat{P}_m \left(2\Delta f_{\max} / \overline{RoCoF}\right) \tag{18}$$

$$R_m^{+} \le \sum_{i\in G(m)} (p_i^{\max} - p_{i,t}) + \sum_{i\in E(m)} \left(p_i^{\mathrm{E,max}} - p_{i,t}^{\mathrm{E}}\right) + \sum_{i\in W(m)} \left(p_{i,t}^{\mathrm{Fore}} - p_{i,t}^{\mathrm{R}}\right) \tag{19}$$

$$R_m^{-} + D_m \Delta f_{\max} \ge -p_{m,t}^{\mathrm{DM}} \tag{20}$$

$$R_m^{-} \le \Delta \hat{P}_m \left(2\Delta f_{\max} / \overline{RoCoF}\right) \tag{21}$$

$$R_m^- \le \sum_{i \in G(m)} \left(p_{i,t} - p_i^{\min} \right) + \sum_{i \in E(m)} \left(p_{i,t}^{\mathrm{E}} - p_i^{\mathrm{E,min}} \right) + \sum_{i \in W(m)} p_{i,t}^{\mathrm{R}} \tag{22}$$

$$\begin{cases} \frac{p_{m,t}^{\mathrm{DM}} f_0}{2H_m} \le \overline{RoCoF} \\ -\frac{p_{m,t}^{\mathrm{DM}} f_0}{2H_m} \le \overline{RoCoF} \end{cases} \tag{23}$$

where the parameters $p_i^{\min}$ and $p_i^{\max}$ denote the lower and upper power limits of generators, respectively; $r_i^{\max}$ and $r_i^{\min}$ represent the ramp-up and ramp-down limits of generators, respectively; $p_i^{\mathrm{E,min}}$ and $p_i^{\mathrm{E,max}}$ denote the lower and upper power limits of energy storage; $E_{i,t}^{\min}$ and $E_{i,t}^{\max}$ are the lower and upper energy limits of energy storage, with their calculation method provided in [24]; Pwt represents the forecasted power of renewable units; H_m denotes the inertia of the microgrid; P_t^{D} is the load demand; and D_m is the damping coefficient. The variables $p_{i,t}$, $p_{i,t}^{\mathrm{E}}$, and $p_{i,t}^{\mathrm{R}}$ denote the power outputs of generators, energy storage, and renewable units, respectively; R_m^+ and R_m^- denote the upward and downward reserves of the microgrid for addressing low-frequency and high-frequency issues, respectively; and $p_{m,t}^{\mathrm{DM}}$ represents the exchanged power with the distribution network, which is positive when power is injected into the microgrid and serves as the source of power imbalance after unintentional islanding.

It should be noted that constraint (17) ensures that when the injected power is positive, the minimum frequency does not exceed the prescribed limit; if the injected power is negative, this constraint becomes redundant. Constraints (18) and (19) impose limits on the upward frequency reserves. Constraints (20)–(22) follow the same logic as (17)–(19) and are therefore not repeated here.

4. Projection-Based Coordinated Scheduling Method for Distribution–Microgrid Systems

In distribution–microgrid systems, each microgrid is subject to strong inter-temporal coupling and heterogeneous device constraints, while the distribution network is further restricted by power flow, line loss, and violation risk constraints. Considering data privacy and scalability, distributed optimization has become the mainstream approach. Classical decomposition–coordination methods can partially alleviate the drawbacks of centralized solutions, but as the number and scale of microgrids increase, these methods often suffer from excessive communication rounds, large data exchanges, sensitivity to penalty parameters and initial values, and even convergence delays. To address these issues, this paper proposes a projection-based coordinated scheduling method for distribution–microgrid systems.

4.1. Definition of Microgrid Feasible Region Projection

Instead of uploading all internal decision variables, each microgrid provides only its low-dimensional projection feasible region (FR) with respect to the boundary power variables that are coupled with the distribution network. Specifically, the high-dimensional feasible region is projected onto the low-dimensional space of boundary power, after which the distribution network determines the power dispatch instructions for each microgrid through a single central optimization.

For ease of notation, the microgrid index is omitted. Let vector $\mathbf{p} = \left[p_1^{\mathrm{DM}}, ..., p_T^{\mathrm{DM}} \right]^{\mathrm{T}}$ denote the DN–MG coupling variables (i.e., the projection operator), and $\mathbf{x}$ denote microgrid decision variables. The high-dimensional feasible region of the microgrid can then be defined as:

$$\Phi = \{ \mathbf{x} | \, \mathbf{A}\mathbf{x} \le \mathbf{b} \} \tag{24}$$

where matrix **A** and vector **b** represent the internal constraint matrix and the right-hand-side vector of the microgrid, respectively. The equality constraints can be equivalently transformed into two inequality constraints.

By projecting the high-dimensional feasible region onto the boundary power **p**, the following low-dimensional feasible region is obtained:

$$\Omega = \{\mathbf{p} | \exists \mathbf{x}, \text{s.t. } \mathbf{A}\mathbf{x} \leq \mathbf{b}, \mathbf{p} = \mathbf{C}\mathbf{x}\} \tag{25}$$

where matrix **C** represents the mapping relationship between variables **x** and **p**.

4.2. Assumption of Power–Energy Boundary

In multi-period problems, the boundary power of a microgrid is constrained not only by the upper and lower limits of single-period outputs but also by the cumulative energy constraints across periods. Therefore, the shape of the projection feasible region can be approximated as jointly determined by the power boundary and the energy boundary. For the purpose of modeling and subsequent approximation, the following assumption is proposed:

Power boundary assumption: At any period t, the boundary power of the microgrid lies between the specified upper and lower limits, that is,

$$\mathbf{p}_{\min} \leq \mathbf{p} \leq \mathbf{p}_{\max} \tag{26}$$

Energy boundary assumption: Over any consecutive time interval, the cumulative sum of the microgrid boundary power should satisfy the energy constraint, that is,

$$E_t^{\min} \leq \sum_{j=1}^{t} p_j \leq E_t^{\max}, \forall t \tag{27}$$

The boundary parameters $\mathbf{p}_{\max}$, $\mathbf{p}_{\min}$, $E_t^{\max}$, and $E_t^{\min}$ can all be obtained by solving an optimization problem [27].

4.3. Inner-Approximation Method

Constraints (26) and (27) together form an outer approximation of feasible region, which can be expressed in the following compact form:

$$\Omega^0 = \{\mathbf{p} | \mathbf{D}\mathbf{p} \leq \mathbf{d}\} \tag{28}$$

However, outer approximation cannot ensure a safe characterization of the microgrid feasible region. To address this, this paper proposes an inner-approximation method based on a leader–follower game. Specifically, the game problem is defined as follows:

$$\begin{aligned} &\min_{\mathbf{p}} \max_{\mathbf{x}} 0 \\ &s.t. \quad \begin{aligned} &\mathbf{A}\mathbf{x} \leq \mathbf{b} \\ &\mathbf{D}\mathbf{p} \leq \mathbf{d} \\ &\mathbf{p} = \mathbf{C}\mathbf{x} \end{aligned} \end{aligned} \tag{29}$$

Within this framework, **p** is regarded as the leader's decision variable, while the follower's decision variables are represented by **x**. The leader aims to identify a "worst-case" solution that lies within set Ω^0 but cannot simultaneously satisfy sets $\mathbf{p} = \mathbf{C}\mathbf{x}$ and $\mathbf{A}\mathbf{x} \leq \mathbf{b}$. If such a solution exists, the follower's maximization problem becomes infeasible, and the optimal value of (29) is negative infinity. Conversely, if no such point exists, the optimal value of (29) equals zero, indicating that set Ω^0 is an inner approximation of set Ω.

By applying dual transformation, problem (29) can be reformulated into the following mixed-integer linear programming (MILP) form:

$$\begin{aligned} \min_{\mathbf{p},\,\boldsymbol{\lambda},\,\boldsymbol{\pi},\,\boldsymbol{\omega},\,\mathbf{s}} \quad & \boldsymbol{\lambda}^{\mathrm{T}}\mathbf{b} - \boldsymbol{\omega}^{\mathrm{T}}\mathbf{d} \\ & \boldsymbol{\omega}^{\mathrm{T}}\mathbf{D} + \boldsymbol{\pi}^{\mathrm{T}} = \mathbf{0} \\ & \boldsymbol{\lambda}^{\mathrm{T}}\mathbf{A} + \boldsymbol{\pi}^{\mathrm{T}}\mathbf{C} = \mathbf{0} \\ & \boldsymbol{\lambda} \geq \mathbf{0} \\ s.t. \quad & \mathbf{0} \leq \boldsymbol{\omega} \leq M\mathbf{s} \\ & \mathbf{0} \leq \mathbf{d} - \mathbf{D}\mathbf{p} \leq M(1-\mathbf{s}) \\ & \mathbf{p} = \mathbf{C}\mathbf{x} \\ & \mathbf{s} \in \{0,1\}^n \end{aligned} \tag{30}$$

where $\boldsymbol{\lambda}$, $\boldsymbol{\omega}$, and $\boldsymbol{\pi}$ are the dual variables; n denotes the dimension of the projection variable $\mathbf{p}$; and M is a sufficiently large positive constant, which is set to 20,000 in this paper.

By solving problem (30), it can be determined whether set Ω^0 is an inner approximation of set Ω. If the objective function value is nonzero, the boundary can be tightened through the following computation by reducing the right-hand-side vector $\mathbf{d}$:

$$(\mathbf{d}_{k+1})_v = \begin{cases} \mathbf{D}\mathbf{p}_k^{\mathrm{bd}}, if\ v \in \Psi_k \\ (\mathbf{d}_k)_v \end{cases} \tag{31}$$

where k denotes the iteration index; v denotes the row index of the active boundary constraint; $\mathbf{p}_k^{\mathrm{bd}}$ represents the feasible point with the minimum distance; and Ψ_k denotes the set of active boundary constraint row indices obtained in the k-th iteration, where the active constraint set is defined as follows:

$$\Psi_k := \{v | \mathbf{D}_v \mathbf{p}_k^* = (\mathbf{d}_k)_v\} \tag{32}$$

where $\mathbf{p}_k^*$ is obtained by solving problem (30).

The minimum-distance feasible point $\mathbf{p}_k^{\mathrm{bd}}$ is obtained by solving the following minimum 2-norm problem:

$$\begin{aligned} & \mathbf{p}_k^{\mathrm{bd}} = \arg\min_{\mathbf{x},\mathbf{p}} \left\| \mathbf{p}_k^* - \mathbf{p} \right\|_2 \\ & s.t. \mathbf{A}\mathbf{x} \leq \mathbf{b}, \mathbf{p} = \mathbf{C}\mathbf{x} \end{aligned} \tag{33}$$

4.4. Overall Procedure of Feasible Region Projection

Based on Sections 4.1–4.3 the inner-approximation procedure of the microgrid feasible region can be summarized as follows:

1. Initialize the iteration index k = 0, and compute the initial boundary parameters $\mathbf{D}$ and $\mathbf{d}$.
2. Solve problem (30). If the objective function value is equal to 0, terminate; otherwise, proceed to the next step.
3. Obtain Ψ_k based on (32).
4. Compute the updated value $\mathbf{p}_k^{\mathrm{bd}}$ according to (33).
5. Tighten the boundary coefficient vector $\mathbf{d}$ using (31).
6. Update $k = k + 1$ and return to Step 2.

In each iteration, the vector $\mathbf{d}$ is guaranteed to be non-increasing in all components, leading to a monotonically shrinking size of Ψ_k. In problem (30), the optimal solution of p is always attained at one of the vertices of its feasible region. Since the feasible region of p is a convex polyhedron with a finite number of vertices, the iterative process will converge in a finite number of iterations.

4.5. Non-Iterative Coordination Optimization Framework for Distribution–Microgrid Systems

After each microgrid projects its feasible region into the reduced-dimensional space, the resulting boundary parameters are transmitted to the distribution network. The distribution network then performs non-iterative coordinated optimization based on this information. The optimization problem is formulated as follows:

$$\begin{aligned} \min \quad & \sum_{t\in T}\sum_{g\in G} c_g^{\mathrm{GEN}} P_{g,t}^{\mathrm{GEN}} + \sum_{t\in T}\sum_{e\in E}\left(c_e^{\mathrm{dch}} P_{e,t}^{\mathrm{dch}} + c_e^{\mathrm{ch}} P_{e,t}^{\mathrm{ch}}\right) + \sum_{t\in T} c_t^{\mathrm{EX}} P_t^{\mathrm{EX}} \\ & \phi(\mathbf{x}_{\mathrm{DN}}) \le \mathbf{0} \\ & \mathbf{x}_{\mathrm{DN,bd},m} = \mathbf{x}_{\mathrm{MG,bd},m}, \forall m \in M \\ & \mathbf{D}_m \mathbf{x}_{\mathrm{MG,bd},m} \le \mathbf{d}_m, \forall m \in M \end{aligned} \tag{34}$$

4.6. Coordinated Scheduling Procedure Between DN and MGs

1. Each microgrid establishes its optimization model incorporating frequency security constraints.
2. Based on the algorithm presented in Section 4.3, each microgrid performs a dimension-reduced projection to obtain its feasible region.
3. Each microgrid submits its projected feasible region to the DN, which performs scheduling optimization according to problem (34).
4. The DN sends the resulting boundary power schedules to each microgrid.
5. Each microgrid conducts internal resource optimization following the received boundary power commands.

5. Case Study

To validate the effectiveness of the proposed scheduling method, case studies are conducted on a modified IEEE-33 bus test system. The load data and line parameters can be found in [24]. The topology of the modified IEEE-33 bus distribution network is shown in Figure 1, which consists of 32 branches, 3 generators, 5 energy storage units, and 3 renewable units. Three microgrids are connected to the distribution network through buses 8, 11, and 25, respectively. This study assumes that each microgrid has a compact electrical structure with negligible internal distances and is therefore modeled as a single-node equivalent system.

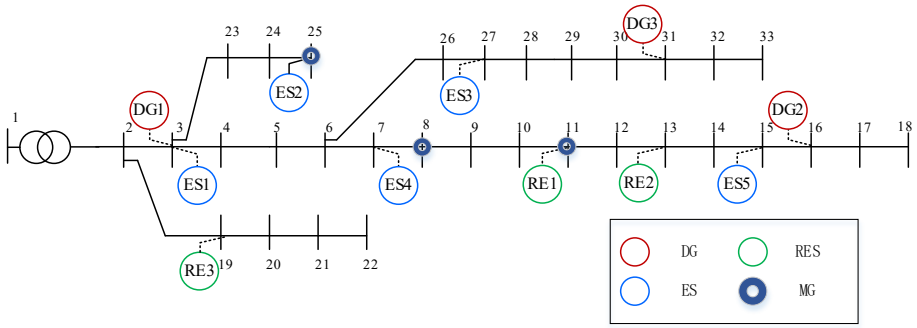


Figure 1. Modified IEEE-33 bus test system.

The scheduling horizon is set to 24 periods with a time step of 1 h. The RoCoF threshold is specified as 0.5 Hz/s, and the maximum frequency deviation threshold is set to 0.5 Hz. For comparison, two scheduling methods are defined as follows.

- M1: DN–MG scheduling without considering microgrid frequency constraints.
- M2: The proposed DN–MG scheduling method with microgrid frequency constraints.

5.1. Comparison of Economic Costs Under Two Scheduling Methods

Table 1 summarizes the total operation costs of the DN–MG system under the two scheduling methods. The results show that, when microgrid frequency constraints are considered in Method M2, the total operating cost increases significantly compared to Method M1, rising from $25,653.37 to $30,596.65, with an increase of about 19.3%. Specifically, the generation cost in M2 is $8598.65, slightly higher than $8079.65 in M1; the energy storage cost increases from $9987.41 to $10,008.99; meanwhile, the cost of power exchange decreases from $–5273.27 to $–3217.22, a reduction of about 39.0%, reflecting the fact that the flexibility of power exchange is constrained, thereby limiting the trading opportunities between the distribution network and the main grid.

Table 1. Operation cost under different dispatch method.

Method	Generation ($)	Energy Storage ($)	Power Exchange ($)	Total Cost ($)
M1	8079.65	9987.41	−5273.27	25,653.37
M2	8598.65	10,008.99	−3217.22	30,596.65

These results indicate that the introduction of frequency constraints reduces the regulating capacity provided by microgrids, forcing the distribution network to rely more on local resources while simultaneously lowering the revenue from power exports to the main grid. Consequently, the overall operating cost increases. This highlights the trade-off between economic efficiency and frequency security in DN–MG coordinated scheduling.

5.2. Comparison of Power Exchange Under Two Scheduling Methods

Figures 2 and 3 illustrate the power exchanges of the three microgrids under Methods M1 and M2, respectively. From the overall trend, both methods exhibit a common feature: except during the midday load peak, the microgrids supply power to the distribution network for most of the day. This indicates that, under a typical daily load profile, microgrids—supported by distributed generation and energy storage—can provide energy to the distribution network in most periods, while during the midday peak they require power imports due to rising local demand. On this basis, the two methods also display notable differences. Under Method M1, since frequency security constraints are not considered, the power exchanges between microgrids and the distribution network are more extensive, with exchange levels approaching 500–1500 kW in certain periods, demonstrating greater flexibility. By contrast, under Method M2, the introduction of frequency security constraints strictly limits the boundary power of microgrids within the range of −750 kW to 250 kW, leading to a significant reduction in the fluctuation of the exchange curves.

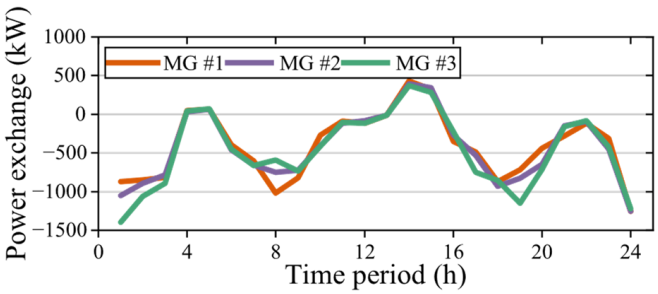


Figure 2. Power exchange between the three microgrids and the distribution network under the M1 method.

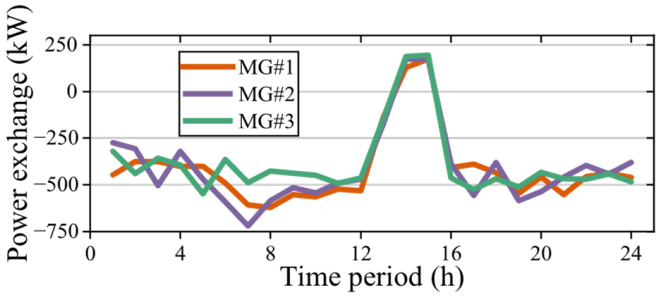


Figure 3. Power exchange between the three microgrids and the distribution network under the M2 method.

These results indicate that frequency constraints effectively suppress excessive power interactions between microgrids and the distribution network, thereby preventing large power imbalances that could trigger frequency violations during unintentional islanding events. In other words, Method M2 improves microgrid operational security at the expense of some flexibility in power exchange.

Moreover, the introduction of frequency security constraints reduces power exchange between the DN and MGs, limiting the flexibility that microgrids can provide to the distribution network. As a result, the DN has less exportable power to the upstream grid, leading to a significant decrease in exchange revenue. Meanwhile, the slight increase in energy-storage cost occurs because the reduction in MG-provided flexibility forces the DN to rely more on its own storage units to balance local demand. However, this increase remains modest since the DN still possesses sufficient internal generation resources to meet most of its load requirements.

5.3. Comparison of Maximum Frequency Deviation Under Two Scheduling Methods

To further validate the effectiveness of the proposed method in ensuring microgrid frequency security, an average system frequency response model [8] is built in Matlab/Simulink 2024a based on the optimized scheduling results. Dynamic simulations are performed for unintentional islanding events occurring at different periods, and the maximum frequency deviations of the three microgrids are compared under the two methods. The results are shown in Figures 4 and 5. As observed, under Method M2 the maximum frequency deviation is consistently suppressed within 0.8 Hz, whereas under Method M1 the deviation reaches as high as 2.5 Hz, indicating significantly weaker frequency stability. It can also be seen that when large power exchanges occur between the microgrids and the distribution network, the post-contingency frequency deviations tend to be larger, reflecting a certain degree of correlation between the two. This explains why, in Method M2, power exchanges are compressed into a smaller range to reduce potential frequency security risks.

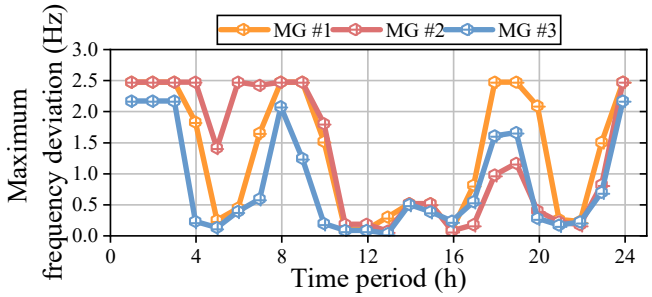


Figure 4. Maximum frequency deviation of three microgrids under M1 dispatch after unintentional islanding.

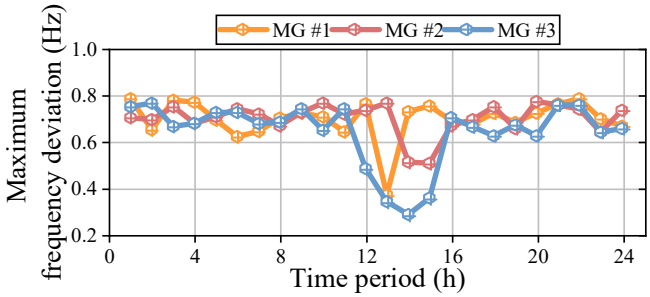


Figure 5. Maximum frequency deviation of three microgrids under M2 dispatch after unintentional islanding.

Overall, these results confirm the effectiveness of the proposed method in enhancing microgrid frequency security. At the same time, they align with the earlier analysis that limiting power exchanges reduces economic efficiency, further highlighting the necessity of balancing security and economic objectives in DN–MG coordinated scheduling.

5.4. Validation of the Effectiveness of Feasible Region Inner Approximation

To further validate the effectiveness of the proposed projection-based DN–MG coordinated scheduling method, a coverage ratio index is introduced as a metric to evaluate the performance of the inner approximation [27]. The coverage ratio is defined as the proportion of feasible dispatch points that satisfy all operational constraints in practice and fall within the inner-approximated feasible region. A value closer to 1 indicates that the inner approximation provides higher coverage of the true feasible region, implying less conservativeness and better approximation accuracy.

Several commonly used projection methods are compared, including the vertex search method [26], multi-parametric programming [14], the box-based inner approximation method [23,24], and the adaptive constraint generation method [17,28]. The results show that the first three methods fail to complete the construction of the microgrid projection feasible region within one hour of computation time, while only the box-based approximation method can provide results within the time limit. This demonstrates that, under temporal coupling and multiple constraints, traditional methods generally suffer from excessive computational complexity and low convergence efficiency.

Table 2 presents a comparison between the proposed method and the box-based inner approximation in terms of coverage ratio and computation time. It can be observed that the coverage ratio of the box method is only 38.68%, whereas the proposed method improves the coverage ratio to 87.62%, significantly enhancing its ability to approximate the true feasible region. This improvement indicates that the proposed method reduces conservativeness while more accurately capturing the power–energy boundary characteristics of microgrids under temporal coupling. The iterative convergence process of the proposed method, as shown in Figure 6, requires only seven iterations to converge, with a total computation time of 180.78 s, demonstrating high computational efficiency that fully meets the requirements of both day-ahead and intra-day scheduling applications.

Table 2. A comparison between the proposed method and the box-based inner approximation method.

Method	Proposed in This Paper	Box-Based Inner Approximation
Cover rate	87.62%	38.68%
CPU time (s)	180.78	32.19

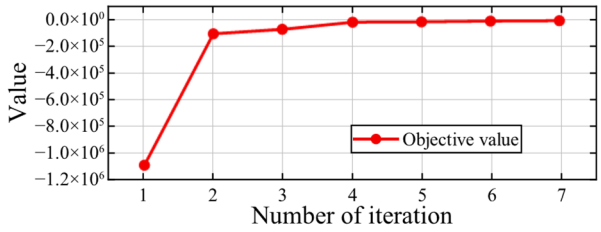


Figure 6. The convergence process of the power–energy boundary-based inner approximation.

It is worth noting that the reported 87.6% coverage ratio represents the extent to which the inner-approximated feasible region captures the true feasible domain. The remaining 12.4% corresponds to feasible operating points that are not included in the constructed approximation. Since the proposed method adopts an inner-approximation framework, all dispatch points within the approximated region are strictly feasible and guarantee frequency-secure operation. Excluding part of the feasible region makes the model more conservative but also more robust, preventing infeasible or unstable dispatch decisions. Therefore, the uncovered portion reflects a deliberate trade-off between conservativeness and completeness, ensuring high reliability in practical coordination scheduling.

In addition, a comparative analysis with the methods in [24–26] is conducted. References [24,25] are based on idealized assumptions of distributed energy resources (DERs), such as neglecting ramp-rate constraints, which limits their applicability to more complex microgrid systems. In contrast, Reference [26] employs a heuristic time-decoupling approach combined with a vertex-search algorithm. Although this method improves computational efficiency to some extent, it requires 68.74 s to complete and achieves only 50.98% coverage, due to the inaccuracy introduced by heuristic time decoupling.

5.5. Scalability

To verify the scalability of the proposed method, the distribution network is expanded to the IEEE 141-bus system, containing 25 microgrids, each equipped with 5–10 distributed energy resources (DERs), and the scheduling horizon is extended to 96 time periods. The results show that our non-iterative coordination method completes the scheduling process within 100 s, whereas the centralized optimization requires 256.84 s due to the large number of variables and constraints. Furthermore, when comparing our inner-approximation-based projection method with the conventional box approximation, the feasible region coverage achieved by our method is 74.98%, compared to 35.98% for the box-based method. It is worth noting that as the number of time periods increases, the dimension of the projection operator also grows, which inevitably reduces the precision of the inner approximation. In future work, we plan to develop enhanced inner-approximation techniques to maintain accuracy under long scheduling horizons.

5.6. Sensitivity Analysis of Linearization Error in the Maximum Frequency Deviation Constraint

The proposed linearized maximum frequency deviation constraint depends on the approximation of τ^*. To evaluate the impact of this approximation, we fix different τ^* values and examine the trade-off between economic performance and frequency security. In the baseline setting, τ^* is approximated as 1 s.

As shown in Table 3, when τ^* = 0.5 s or 1 s, the frequency security requirement is always satisfied, whereas for τ^* = 2 s or 4 s, frequency violations occur despite lower total operating costs. This result demonstrates that underestimating τ^* enhances robustness at the expense of slight conservativeness, thereby validating the practicality of the proposed linearization approach.

Table 3. Total operation cost and frequency security performance under different τ^* approximations.

τ^*	0.5	1	2	4
Total cost ($)	30,824.31	30,596.65	30,247.44	30,098.45
Frequency security guarantee	Yes	Yes	No	No

6. Conclusions

This paper proposes a projection-based coordinated scheduling method for distribution–microgrid systems under microgrid frequency security constraints. First, the maximum frequency deviation constraint of microgrids under unintentional islanding is derived from the frequency response curve and linearized for embedding into the optimization model. Then, an inner-approximation construction method based on power–energy boundaries is introduced, enabling non-iterative DN–MG coordinated scheduling. Finally, case studies on a modified IEEE-33 bus system with three microgrids are conducted, and the following conclusions are drawn:

1. Frequency security constraints significantly affect power exchange and economic performance. Without frequency constraints, microgrids exhibit larger power exchanges with the distribution network and better economic outcomes, but at the cost of higher frequency risks. With the inclusion of frequency constraints, the exchange range is compressed, system flexibility decreases, and economic efficiency is partially sacrificed, but frequency stability during unintentional islanding is effectively guaranteed.
2. Frequency constraints are essential in DN–MG coordination. Simulation results show that, without frequency constraints, the maximum frequency deviation of microgrids can reach 2.5 Hz, posing severe instability risks. In contrast, under the proposed method, the maximum deviation is suppressed within 0.8 Hz, significantly enhancing system security.
3. The proposed method outperforms box-based inner approximation. Compared with the box method, the coverage ratio is improved from 38.68% to 87.62%, substantially reducing conservativeness. Moreover, the proposed method achieves fast iterative convergence, completing computation within hundreds of seconds. It avoids the slow convergence and heavy communication burden of ADMM while overcoming the privacy and scalability limitations of centralized scheduling, thus demonstrating strong potential for practical engineering applications.

In future work, stochastic factors such as renewable generation uncertainty and load fluctuations will be incorporated into the microgrid model to further enhance the robustness and practicality of the proposed coordinated scheduling framework.

Author Contributions: Methodology, X.S. and W.W.; Formal analysis, L.G.; Data curation, M.S.; Writing—original draft, X.T.; Writing—review and editing, M.L. All authors have read and agreed to the published version of the manuscript.

Funding: Research and Application of Cloud-Edge Collaborative Scheduling Decision Support Technology for Low-Voltage Distribution Networks Under Incomplete Data Conditions (CX-YF 2024-03). Funder: State Grid Tianjin Electric Power Company.

Data Availability Statement: The original contributions presented in this study are included in the article. Further inquiries can be directed to the corresponding authors.

Conflicts of Interest: Authors Xingwang Song, Mingjun Sun and Xinyu Tong were employed by the company State Grid Tianjin Chengxi Electric Power Supply Branch. Author Lingxu Guo was

employed by the company State Grid Tianjin Electric Power Company. The remaining authors declare that the research was conducted in the absence of any commercial or financial relationships that could be construed as a potential conflict of interest.

References

1. Khodayar, M.E.; Barati, M.; Shahidehpour, M. Integration of high reliability distribution system in microgrid operation. *IEEE Trans. Smart Grid* **2012**, *3*, 1997–2006. [CrossRef]
2. Van Impe, J.F.M.; Léonard, G.; Bhonsale, S.S.; Polańska, M.E.; Logist, F. Multi-objective Optimization of Steam Cracking Microgrid for Clean Olefins Production. *Syst. Control. Trans.* **2025**, *4*, 837–843. [CrossRef]
3. Muhtadi, A.; Pandit, D.; Nguyen, N.; Mitra, J. Distributed energy resources based microgrid: Review of architecture, control, and reliability. *IEEE Trans. Ind. Appl.* **2021**, *57*, 2223–2235. [CrossRef]
4. Zhou, K.; Yang, S.; Chen, Z.; Ding, S. Optimal load distribution model of microgrid in the smart grid environment. *Renew. Sustain. Energy Rev.* **2014**, *35*, 304–310. [CrossRef]
5. Liang, Z.; Chung, C.Y.; Zhang, W.; Wang, Q.; Lin, W.; Wang, C. Enabling High-Efficiency Economic Dispatch of Hybrid AC/DC Networked Microgrids: Steady-State Convex Bi-Directional Converter Models. *IEEE Trans. Smart Grid* **2025**, *16*, 45–61. [CrossRef]
6. Cai, S.; Xie, Y.; Zhang, Y.; Bao, W.; Wu, Q.; Chen, C.; Guo, J. Frequency constrained proactive scheduling for secure microgrid formation in wind power penetrated distribution systems. *IEEE Trans. Smart Grid* **2025**, *16*, 989–1002. [CrossRef]
7. Wen, Y.; Lin, X. Minimum Inertia Requirement Assessment of Microgrids in Islanded and Grid-connected Modes. *Proc. CSEE* **2021**, *41*, 2040–2052. [CrossRef]
8. Wen, Y.; Chung, C.Y.; Liu, X.; Che, L. Microgrid dispatch with frequency-aware islanding constraints. *IEEE Trans. Power Syst.* **2019**, *34*, 2465–2468. [CrossRef]
9. Chu, Z.; Zhang, N.; Teng, F. Frequency-constrained resilient scheduling of microgrid: A distributionally robust approach. *IEEE Trans. Smart Grid* **2021**, *12*, 4914–4925. [CrossRef]
10. Nakiganda, A.M.; Aristidou, P. Resilient microgrid scheduling with secure frequency and voltage transient response. *IEEE Trans. Power Syst.* **2022**, *38*, 3580–3592. [CrossRef]
11. Wang, Y.; Wu, L.; Wang, S. A fully-decentralized consensus-based ADMM approach for DC-OPF with demand response. *IEEE Trans. Smart Grid* **2016**, *8*, 2637–2647. [CrossRef]
12. Ma, Z.; Zhou, Y.; Zheng, Y.; Yang, L.; Wei, Z. Distributed robust optimal dispatch of regional integrated energy systems based on ADMM algorithm with adaptive step size. *J. Mod. Power Syst. Clean Energy* **2023**, *12*, 852–862. [CrossRef]
13. Rajaei, A.; Arowolo, O.; Cremer, J.L. Learning-Accelerated ADMM for Stochastic Power System Scheduling with Numerous Scenarios. *IEEE Trans. Sustain. Energy* **2025**, *16*, 2701–2713. [CrossRef]
14. Lin, W.; Yang, Z.; Yu, J.; Jin, L.; Li, W. Tie-line power transmission region in a hybrid grid: Fast characterization and expansion strategy. *IEEE Trans. Power Syst.* **2019**, *35*, 2222–2231. [CrossRef]
15. Lin, W.; Yang, Z.; Yu, J.; Yang, G.; Wen, L. Determination of transfer capacity region of tie lines in electricity markets: Theory and analysis. *Appl. Energy* **2019**, *239*, 1441–1458. [CrossRef]
16. Lin, W.; Yu, J.; Yang, Z.; Wang, X. Fast probabilistic optimal power flow based on modified multi-parametric programming. In Proceedings of the 2020 International Conference on Probabilistic Methods Applied to Power Systems (PMAPS), Liege, Belgium, 18–21 August 2020; IEEE: New York, NY, USA, 2020; pp. 1–6.
17. Wei, W.; Liu, F.; Mei, S. Real-time dispatchability of bulk power systems with volatile renewable generations. *IEEE Trans. Sustain. Energy* **2015**, *6*, 738–747. [CrossRef]
18. Zhang, Y.; Chen, C.; Liu, G.; Hong, T.; Qiu, F. Approximating trajectory constraints with machine learning–microgrid islanding with frequency constraints. *IEEE Trans. Power Syst.* **2020**, *36*, 1239–1249. [CrossRef]
19. Xu, D.; Liu, Z.; Hou, K.; Wei, X.; Jia, H.; Wu, Z.; Guan, L. Distributionally Robust Frequency Constrained Low-carbon Scheduling Considering Flexibility of Carbon Capture Power Plants. *Energy* **2025**, *332*, 137171. [CrossRef]
20. Xu, D.; Wu, Z. Enhanced frequency aware microgrid scheduling towards seamless islanding under frequency support of heterogeneous resources: A distributionally robust chance constrained approach. *Int. J. Electr. Power Energy Syst.* **2024**, *162*, 110310. [CrossRef]
21. Li, K.; Ai, X.; Fang, J.; Cui, S.; Feng, Y.; Liu, D.; Gu, P.; Qiu, W.; Wen, J. Frequency security constrained robust unit commitment for sufficient deployment of diversified frequency support resources. *IEEE Trans. Ind. Appl.* **2023**, *60*, 1725–1737. [CrossRef]
22. Liu, L.; Li, W.; Ba, Y.; Shen, J.; Jin, C.; Wen, K. An analytical model for frequency nadir prediction following a major disturbance. *IEEE Trans. Power Syst.* **2020**, *35*, 2527–2536. [CrossRef]
23. Hengxian, L.; Kaiyuan, H.; Lei, C.; Deming, X.; Yong, M.; Shuang, Q.; Bowen, Z. Optimization model of high-frequency second defense line of generator tripping based on frequency safety constraints. In *IOP Conference Series: Earth and Environmental Science, Proceedings of the 2020 4th International Workshop on Advances in Energy Science and Environment Engineering, Hangzhou, China, 10–12 April 2020*; IOP Science: Bristol, UK, 2020; Volume 512, p. 012108. [CrossRef]

24. Zhang, R.; Zhang, Y.; Zou, Y.; Jiang, T.; Li, X. Privacy-Preserving Cooperative Optimal Operation for Reconfigurable Multimicrogrid Distribution Systems: A Noniterative Distributed Optimization Approach. *IEEE Trans. Ind. Inform.* **2025**, *21*, 5766–5776. [CrossRef]
25. Wen, Y.; Hu, Z.; He, J.; Guo, Y. Improved inner approximation for aggregating power flexibility in active distribution networks and its applications. *IEEE Trans. Smart Grid* **2023**, *15*, 3653–3665. [CrossRef]
26. Hao, P.; Huang, C.; Wang, C.; Li, K.; Tan, Z. Non-Iterative Coordinated Optimal Dispatch of Distribution System and Microgrids via Fast Approximation Equivalent Projection. *IEEE Trans. Smart Grid* **2025**, *16*, 3934–3948. [CrossRef]
27. Wang, S.; Wu, W. Aggregate flexibility of virtual power plants with temporal coupling constraints. *IEEE Trans. Smart Grid* **2021**, *12*, 5043–5051. [CrossRef]
28. Liu, Y.; Li, Z.; Wei, W.; Zheng, J.H.; Zhang, H. Data-driven dispatchable regions with potentially active boundaries for renewable power generation: Concept and construction. *IEEE Trans. Sustain. Energy* **2021**, *13*, 882–891. [CrossRef]

Disclaimer/Publisher's Note: The statements, opinions and data contained in all publications are solely those of the individual author(s) and contributor(s) and not of MDPI and/or the editor(s). MDPI and/or the editor(s) disclaim responsibility for any injury to people or property resulting from any ideas, methods, instructions or products referred to in the content.